Hybrid Thin Film Antenna for Automotive Radar at 79 GHz

Osama Khan, Johannes Meyer, Klaus Baur, and Christian Waldschmidt, *Senior Member, IEEE*

***Abstract*— A novel hybrid approach to designing multilayer antennas for automotive radar using a thin single layer printed circuit board and multilayer thin films is presented in this paper. A new substrate integrated waveguide (SIW) slot fed stacked grid antenna element is designed using this approach. The flexibility of this approach in designing antenna arrays is shown by integrating the same antenna element with three different feed networks based on SIW, grounded coplanar waveguide (GCPW), and microstrip (MS) transmission lines. The antenna is designed to operate in the frequency band between 77 and 81 GHz for automotive radar. Measurement results on 1 × 4 arrays show an impedance matching bandwidth and a realized gain of 7.8% (76.3–82.5 GHz) and 9.2 dBi, respectively, for SIW feed antenna, 11.3% (76.3–85.5 GHz) and 10.7 dBi, respectively, for GCPW feed antenna, and 11.3% (75.7–84.8 GHz) and 12.1 dBi, respectively, for MS feed antennas. The proposed antenna can be used for medium- and short-range automotive radar applications.**

***Index Terms*— Automotive radar, grid array antenna, grounded coplanar waveguide (GCPW), microstrip (MS), single-layer, substrate integrated waveguide (SIW), thin films, wideband antenna array.**

I. Introduction

MILLIMETER waves have received a lot of interest in both the academic and research community recently. Development of high precision manufacturing technologies, coupled with regulations supporting the use of millimeter-wave spectrum for commercial applications has enabled the development of sensor and communication systems employing millimeter waves. An important component of these systems, the antenna has been the subject of many research investigations. Antenna designs for the 60 GHz unlicensed short-range band [1]–[6] for point-to-point communication links, as well as automotive radar at 24 [7] and 77 GHz bands [8]–[12] among other applications have been extensively researched.

Cost effective antenna arrays with high gain and large bandwidth are the preferred choice for many millimeter-wave applications. Hence, considerable effort has been made to increase the antenna gain and impedance matching bandwidth without substantially increasing manufacturing costs and complexity. Single layer printed circuit board (PCB) antenna designs are the simplest to manufacture. However, integrating the feed network and radiating elements on a single layer generally requires a compromise between radiation and power distribution properties. Increasing substrate thickness, or employing a lower dielectric permittivity substrate enables a wideband antenna operation. This comes, however, at the expense of increased substrate waves and losses in the feed network [13]. Single layer designs have employed parasitic elements and innovative radiating elements [14] to increase the impedance matching bandwidth.

Multilayer antenna designs provide greater flexibility and improved performance in terms of antenna element and feed network design. Using vertically stacked multiple antenna or impedance matching elements, increased impedance matching bandwidth can be achieved. For example, stacked antennas [15] and multilayer slot backed antennas [16] make use of staggered resonances of individual elements to increase the overall impedance matching bandwidth. Separate layers for feed networks and radiating elements allow optimal choice of substrate material and thickness for each purpose independently. Additionally, complex feed networks can be implemented, especially for large arrays, when multilayer antenna designs are used.

Conventional multilayer PCB technology [17]–[19], as well as low-temperature cofired ceramic [20] technology have been used to realize many multilayer antenna designs. These are complex to manufacture and come with increased costs. Recently, there have been multilayer designs where the individual layers are manufactured using single layer PCB technology and then stacked together using alignment pins and screws [21]. Such multilayer antenna designs are cost-effective as they can be manufactured using single layer manufacturing techniques. Tolerances in PCB alignment or air gaps between the layers can, however, result in performance degradation. Alignment pins and screws required in such designs are also not suitable for robust large-scale manufacture. Another approach uses conductive bonding films with apertures for stacking multiple substrate layers [22], [23]. While this approach is low cost, it also suffers from PCB alignment issues for large-scale manufacturing.

In this paper, a new approach to designing multilayer antennas on single layer PCBs is shown. The approach makes use of thin films that house the complete antenna element on them. Using thin films instead of multilayer PCBs provides the flexibility and performance of multilayer antennas without the requirements or costs of thick substrates or complex multilayer feed networks. Additionally, for automotive radar applications,

Manuscript received February 27, 2017; revised July 3, 2017; accepted July 27, 2017. Date of publication August 17, 2017; date of current version October 5, 2017. *(Corresponding author: Osama Khan.)*

O. Khan, J. Meyer, and K. Baur are with Robert Bosch GmbH, Chassis Systems Control, 71229 Leonberg, Germany (e-mail: osama.khan@de.bosch.com).

C. Waldschmidt is with the Institute of Microwave Engineering, University of Ulm, 89081 Ulm, Germany.

Color versions of one or more of the figures in this paper are available online at http://ieeexplore.ieee.org.

Digital Object Identifier 10.1109/TAP.2017.2741024

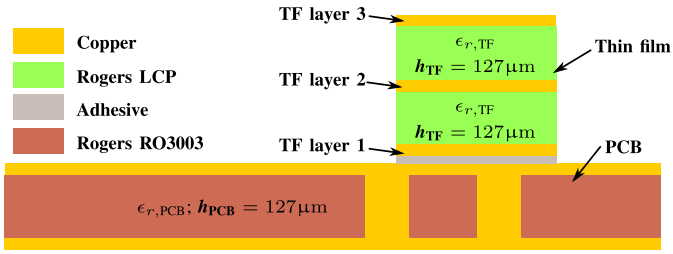

Fig. 1. Cross section of the hybrid multilayer antenna.

this approach eases the manufacturing of sensors, since active elements such as monolithic microwave integrated circuit packages can be placed on the PCB top layer using conventional techniques [24]. Using the thin-film approach, a novel stacked grid antenna element for automotive radar frequency range of 77–81 GHz is presented here. The flexibility of this approach is shown by designing different transmission line feed networks using the same radiating element. The structure of this paper is as follows. In Section II, the structure and manufacturing aspects are described for a hybrid multilayer antenna based on thin films and single layer PCBs. The stacked grid element design is studied and developed in Section III. The effect of positioning tolerance on the antenna performance is also simulated. Section IV describes the feed network designs based on substrate integrated waveguide (SIW), grounded coplanar waveguide (GCPW), and microstrip (MS) transmission lines. Measurement results are presented and discussed in Section V and a conclusion is given in Section VI.

II. Hybrid Multilayer Antenna

A hybrid multilayer antenna layer stackup is shown in Fig. 1. It consists of a large single layer PCB with a smaller thin film attached to it. The thin film itself consists of two substrate layers. In an array design, multiple thin films are attached to the PCB. Both the PCB and thin films are manufactured separately, and they are attached together as the last manufacturing step. The feed network is present on the single layer PCB, while the antenna element is designed on each thin film. A thin single layer PCB with a substrate thickness of $\boldsymbol{h_{\mathrm{PCB}}} = 127\ \mu$m is used, which corresponds to $0.03\ \lambda_0$, where λ_0 is the free space wavelength at 77 GHz. Rogers RO3003 is used as the PCB substrate, with $\epsilon_{r,\mathrm{PCB}} = 3$. A low-loss feed network is designed on the PCB. The feed network on the PCB includes coupling structures to the thin film. Since the thin film is attached to the PCB as a separate step, electrical coupling structures, such as wires or vias, are not a mechanically suitable option to couple the energy. Hence, slots are used as coupling structures. The radiating elements are located on a multilayer thin-film structure. The thin film is constructed using Rogers Ultralam 3850 liquid crystalline polymer laminates and bondply with $\epsilon_{r,\mathrm{TF}} = 3.0$ to form a three metallic (or a two substrate) layer structure with a substrate thickness of $\boldsymbol{h_{\mathrm{TF}}} = 127\ \mu$m each. The parasitic and primary radiating elements are located on the top (layer 3) and middle (layer 2) metallic layer of the thin film, respectively. The bottom metallic layer (layer 1) is etched off except for alignment structures that facilitate the placement of the thin film on the PCB. The top layer of the PCB below the radiating element is metallized and functions as the ground plane for the antenna. The radiating properties of the antenna are thus determined by the thin-film substrate layers, which enables independent design of the feed network and radiating element.

The thin film is attached to the PCB at the radiating position to realize the antenna. The positioning of the thin film needs to be accurate to achieve the required coupling between the slot and radiating elements. Thin-film positioning is achieved using a die bonder [25]. An epoxy-based nonconductive paste adhesive [26] with a thickness of about 10 μm is first deposited by the integrated dispenser of the die bonder at the position where the thin film will be placed. Alignment structures on the bottom layer of the thin film as mentioned earlier, as well as similar structures on the PCB enable an automatic accurate positioning using the pick and place head and integrated camera of the die bonder. A high positioning accuracy of $\pm 7\ \mu$m in the x- and y-axes can be achieved using this process.

III. Single Element Design

The grid array antenna, introduced by Kraus [27] as a wire antenna has been investigated as an MS-based antenna for millimeter-wave antennas [5], [7], [28]–[30]. In all its manifestations until now, the antenna has consisted of many rectangular grid elements that form either a linear or a rectangular array antenna. In this paper, a radiating element based on a double grid element is studied, and using parasitic elements, a new stacked grid antenna configuration is described. Stacking parasitic elements on top of radiating elements has been classically used for MS patch antennas [31]. An additional resonance is achieved due to the parasitic stacked element. This improves the impedance bandwidth of the antenna.

Due to its orientation in a possible implementation in automotive radar, the stacked grid element is characterized as vertically polarized. Antennas with different linear polarizations, such as vertical, horizontal, or 45° tilted polarization have been used for commercial automotive radar. Antenna polarization is chosen due to different considerations, with signal interference between multiple sensors being an important one. A main argument for the use of 45° tilted polarization is that it reduces signal interference from other automotive radar [32]. However, this is not an efficient way of reducing interference, since both radars can have the same tilted polarization and still have interference. A better approach is to use digital beamforming techniques to dynamically reduce interference [33].

The antenna structure, based on the multilayer thin film and PCB layer stackup described earlier, is shown in Fig. 2. A layerwise geometry of this element with all geometrical parameters is shown in Fig. 3. It consists of a shorted SIW of width ***a*** on a single layer PCB, with an off-center longitudinal slot of length ***sl*** at a distance ***sdt*** from the shorting wall to transfer energy to the thin film. A matching via (with distances ***mdl*** and ***msd*** from the via wall and coupling slot, respectively) is used in the SIW to improve the impedance bandwidth of the coupling structure. The slot couples to the MS line on the thin film layer 2. The MS line (with width ***cw*** and length ***cl***) feeds the double grid element in parallel. Due to

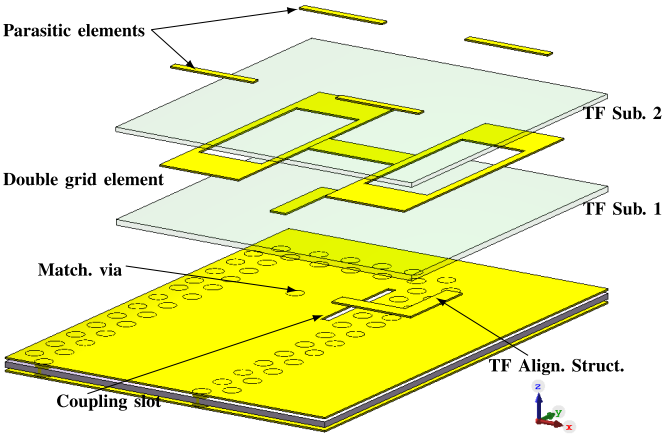

Fig. 2. Geometry of the stacked grid antenna.

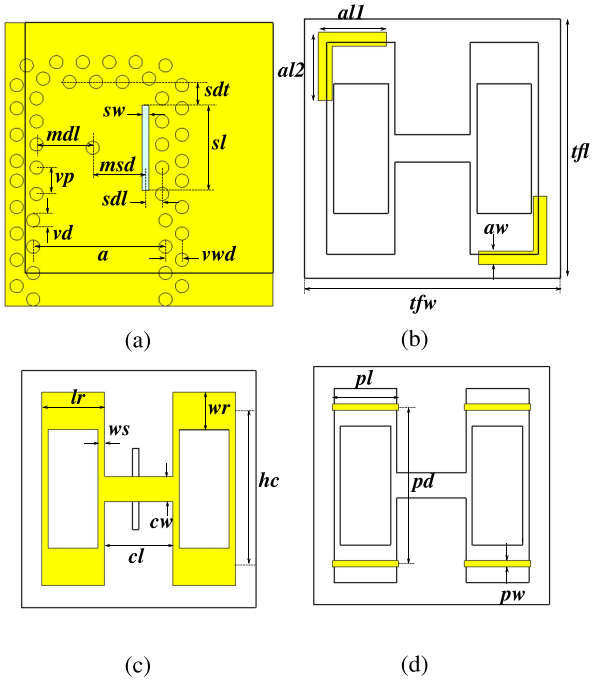

Fig. 3. Top view of the stacked grid antenna geometry. (a) PCB top layer. (b) Thin film layer 1. (c) Thin film layer 2. (d) Thin film layer 3.

TABLE I

OPTIMIZED GEOMETRICAL PARAMETERS FOR A SINGLE ELEMENT. ALL DIMENSIONS IN mm

sw	*sdt*	*mdl*	*msd*	*sl*	*vp*	*vd*	*a*
0.10	0.35	0.85	0.80	1.30	0.40	0.20	2.00
vwd	*al1*	*al2*	*tfl*	*tfw*	*aw*	*lr*	*ws*
0.25	1.00	1.00	3.75	3.80	0.20	1.00	0.10
wr	*cw*	*hc*	*cl*	*pl*	*pd*	*pw*	-
0.60	0.40	2.50	1.10	1.05	2.50	0.10	-

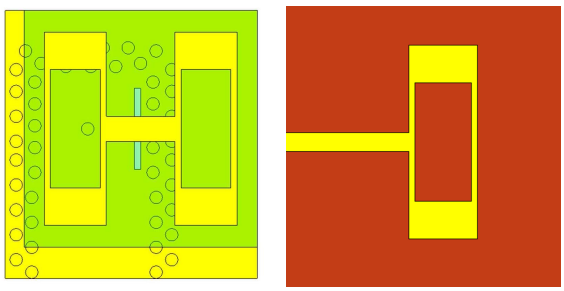

Fig. 4. (a) SIW fed double grid antenna. (b) MS fed single grid antenna.

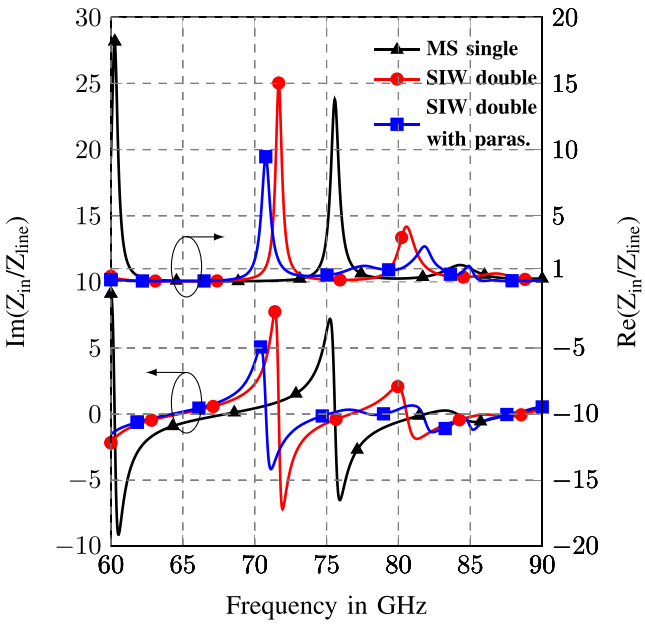

Fig. 5. Comparison of $Z_{\text{in}}/Z_{\text{line}}$ for different grid element configurations.

the coupling mechanism, the grid elements radiate in phase without any additional line length [12]. On the thin film layer 3, rectangular parasitic elements (with length ***pl*** and width ***pw***) are located above the radiating edges of the grid elements and they help improve the impedance bandwidth of the antenna. This completes the design of a single thin-film radiating element. The optimized geometrical parameters for the SIW and radiating element are shown in Table I.

To help understand the impedance bandwidth improvements of the proposed structure, the SIW slot double grid element with parasitic elements (shown in Fig. 3) is compared with the single MS fed grid element as well as the SIW slot fed grid element without the parasitic elements. These antennas are shown in Fig. 4. To this end, the real and imaginary components of the ratio of input impedance Z_{in} to transmission line impedance Z_{line} is plotted for all three configurations in Fig. 5. For the MS fed single grid element, three electrical resonances at 61, 76, and 84 GHz can be seen. The first resonance is outside the working frequency range of the antenna, and it is disregarded. The second resonance has a large impedance ratio Re $(Z_{\text{in}}/Z_{\text{line}})$ of more than 10. The third resonance has a smaller impedance ratio of around 1; hence, the antenna is matched to the transmission line for a small impedance bandwidth. The SIW slot fed double grid element has resonances at 72, 81, and 86 GHz. However, due to high impedance ratio Re $(Z_{\text{in}}/Z_{\text{line}})$ of the first two

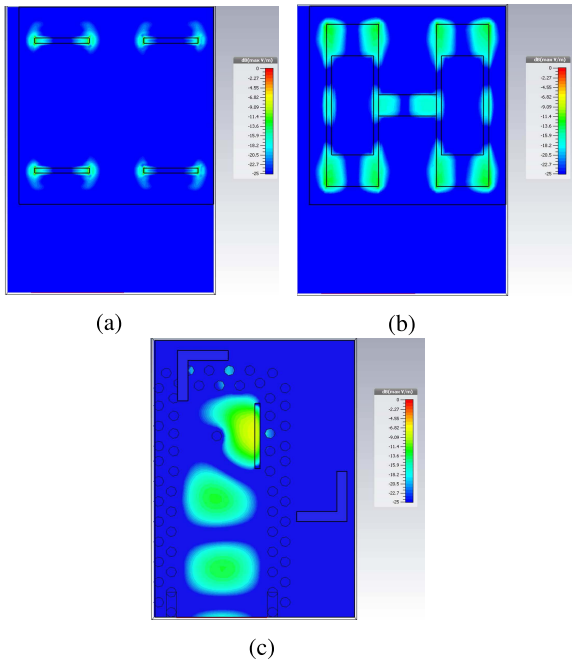

Fig. 6. Electric field distribution for the stacked grid antenna. (a) E-field TF layer 3. (b) E-field TF layer 2. (c) E-field TF layer 1.

resonances, it is also only matched to the third resonance. Adding parasitic elements to the structure results in another resonance at 77 GHz. Additionally, the impedance ratio of the resonance previously at 81 GHz decreases and the resonance shifts to a slightly higher frequency. Due to these effects, the impedance ratios Re ($Z_{\text{in}}/Z_{\text{line}}$) and Im ($Z_{\text{in}}/Z_{\text{line}}$) remain around 1 and 0, respectively, from 76 to 82 GHz for the SIW slot fed double grid with parasitic element. This enables a larger impedance matching bandwidth for this radiating element.

The electric field distribution on different layers of the stacked grid antenna is shown in Fig. 6. It can be seen that the shorted SIW mode on the PCB in Fig. 6(c) is coupled to connecting line between the double grid element on the thin film. After traveling to the radiating edges of the double grid element in Fig. 6(b), the energy is then radiated. Energy is also coupled to the parasitic elements in Fig. 6(c), located above the radiating edges of the double grid element. These also radiate and improve the impedance bandwidth, as described earlier.

The reflection coefficient of the single antenna is shown in Fig. 7. It can be seen that the reflection coefficient is lower than -10 dB for a frequency range from 76 to 82 GHz. Also shown is the broadside realized gain, which shows a maximum broadside gain of 11 dBi at 79 GHz and a 3 dB gain bandwidth of about 7 GHz. The radiation pattern in the E-plane and H-plane are shown in Fig. 8. A broadside radiation pattern is achieved, with cross-polarized radiation suppression of more than 30 dB at broadside. In the E-plane, a slight asymmetry is seen in the radiation pattern due to the offset placement of the thin film over the SIW. The antenna has a broadside H-plane beamwidth of 43° and E-plane beamwidth of 49° at 78 GHz.

Parameters that mainly determine the SIW coupling and frequency response of the single element are varied and shown

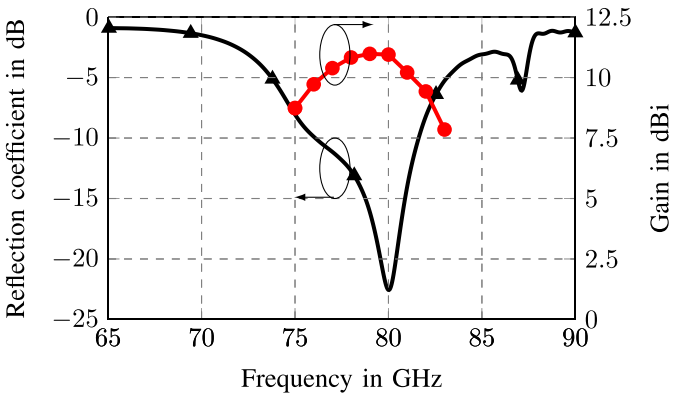

Fig. 7. Reflection coefficient and realized gain of single element.

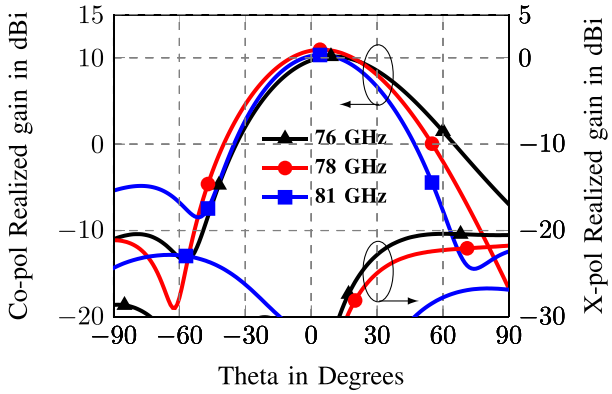

(a)

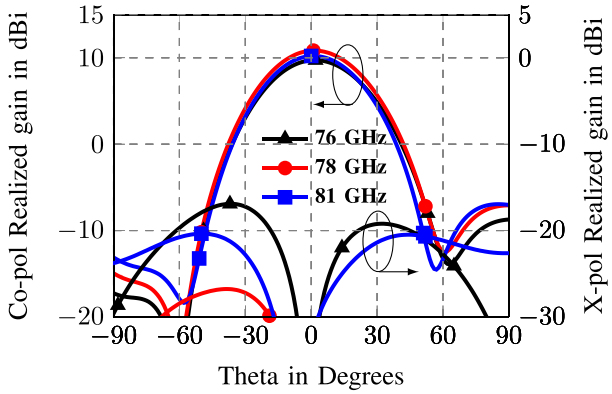

(b)

Fig. 8. Single element simulated far-field results. (a) Realized gain E-plane. (b) Realized gain H-plane.

in Fig. 9. These include the length of the radiating edge of the grid element ***lr***, the SIW coupling slot length ***sl***, and the parasitic element length ***pl***.

In Section III, it was mentioned that the thin film is placed on the PCB using a die bonder [25] with very low positioning error (± 7 μm in the x- and y-axes). For series production with high volume, standard surface-mount technology pick and place machines are used for automotive radar PCB assembly. Depending on the machines used, these errors can range from ± 30 to ± 50 μm in the x- and y-axes. The effect of positioning tolerances on the coupling between the PCB and

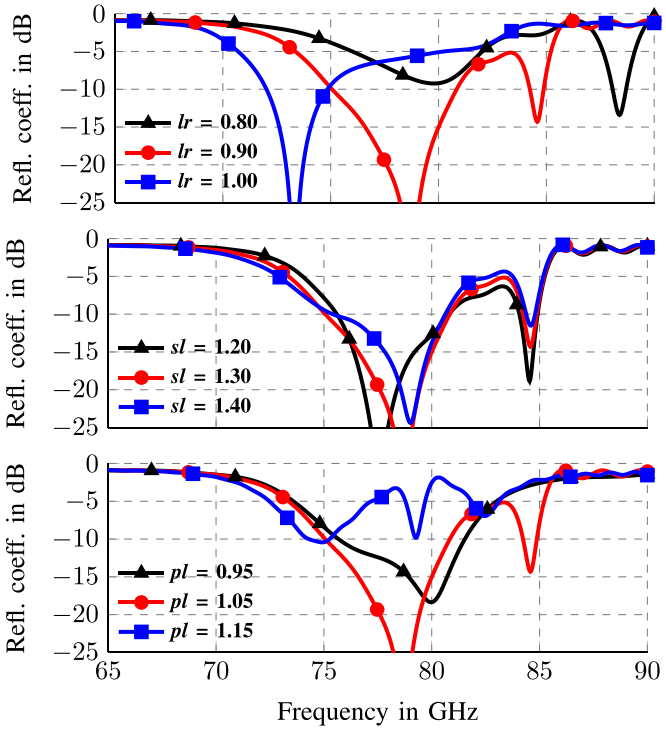

Fig. 9. Parametric analysis of single antenna element. All other dimensions are as listed in Table I.

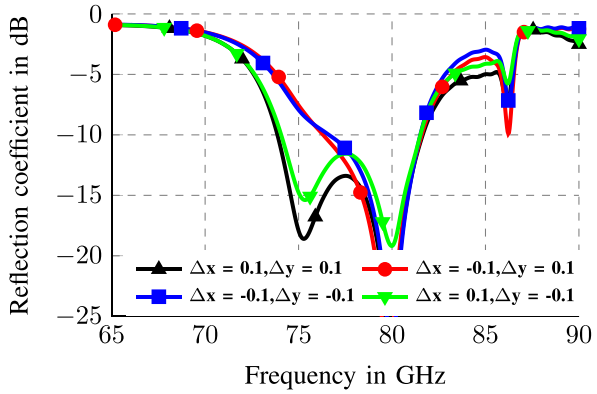

Fig. 10. Reflection coefficient single element with thin-film positioning errors.

thin film is simulated. Positioning errors of ±0.1 mm are included in the simulations. Reflection coefficient results for these simulations are shown in Fig. 10. The different curves show the effect of simultaneous positioning errors in the x- and y-axes. It can be seen that even with positioning errors in both the axes simultaneously, the reflection coefficient is lower than −10 dB for a frequency range of 76.6–81.5 GHz over all values. Although far-field results are not shown, they also vary negligibly from the nominal results due to positioning errors.

IV. Feed Network

To demonstrate the flexibility of array design using the proposed antenna element, linear corporate feed networks using three different transmission line types were designed. The same thin-film antenna element was used to create the

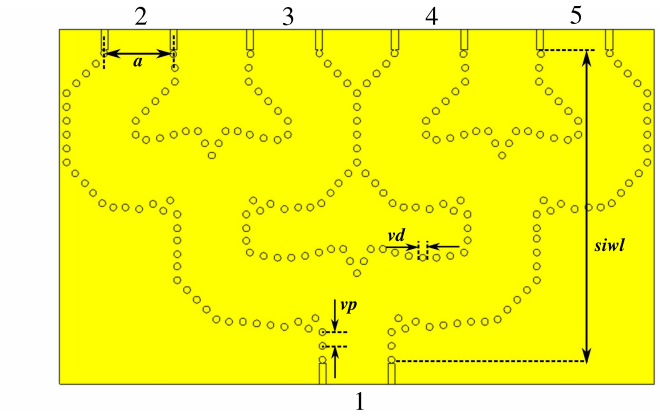

(a)

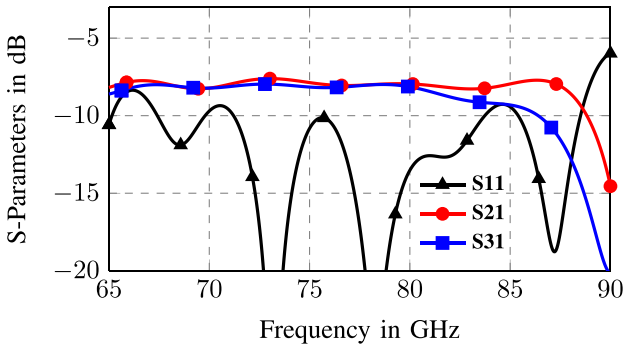

(b)

Fig. 11. SIW feed network geometry and performance. (a) Geometry. (b) Simulated performance.

antenna array using these feed networks. The feed networks are designed on a single layer PCB and terminate in the SIW that feeds the antenna element as described earlier. Optimized geometrical parameters for the feed networks described in the following are listed in Table II.

A. Substrate Integrated Waveguide Feed Network

A feed network based on SIW transmission line was designed. A symmetric design is employed with a two equal stage power division that results in four outputs with equal power distribution. A compact design was implemented with the intention to reduce the size and dielectric losses due to the feed network. A single row of vias was used in the SIW in order to reduce space. The condition in [34] for negligible leakage loss is fulfilled with a single via row, considering the choice of via diameter and pitch ***vd*** and ***vp***, respectively. The design and the performance of the feed network are shown in Fig. 11. The size of the SIW feed network is related to the length ***siwl***, which is 11.1 mm for the SIW feed network. The reflection coefficient stays below −10 dB for the frequency of operation. Since it is a symmetric design, transmission results for ports 2 and 3 are shown, which show equal power distribution for the operating frequency range.

B. Grounded Coplanar Waveguide Feed Network

The GCPW feed network was designed symmetrically with two-stage power division that results in four outputs. The first

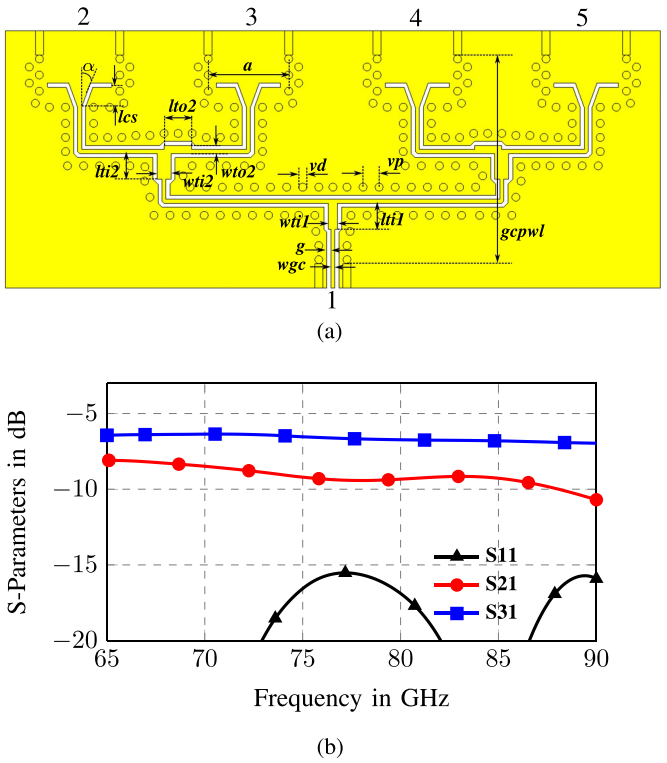

Fig. 12. GCPW feed network geometry and performance. (a) Geometry. (b) Simulated performance.

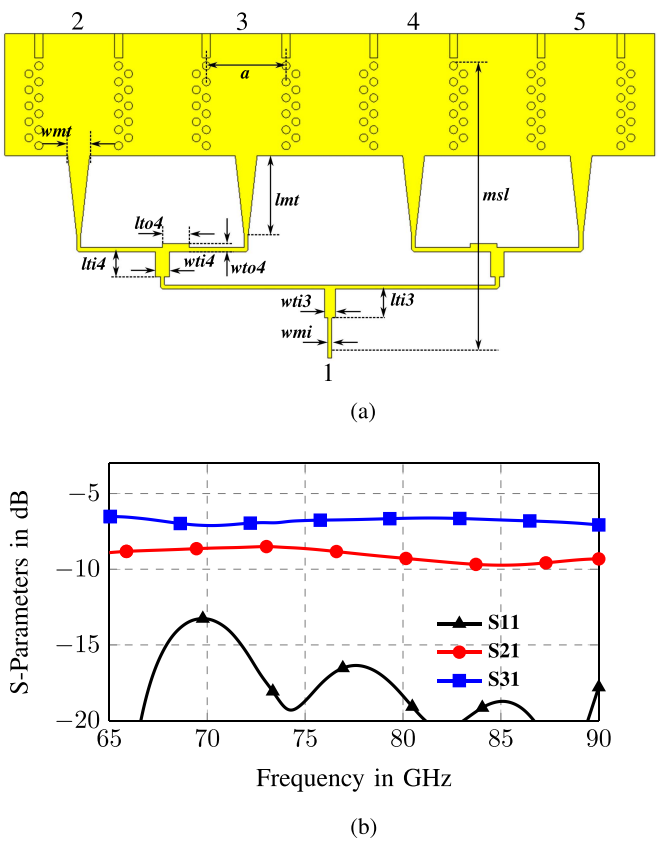

Fig. 13. MS feed network geometry and performance. (a) Geometry. (b) Simulated performance.

TABLE II
OPTIMIZED GEOMETRICAL PARAMETERS FOR FEED NETWORKS. ALL LENGTH DIMENSIONS IN mm

siwl	α	***lcs***	***lti1***	***wti1***	***wti2***	***lti2***
9.05	20°	0.55	0.65	0.23	0.35	0.63
lto2	***wto2***	***g***	***wgc***	***gcpwl***	***wmt***	***lmt***
0.68	0.20	0.10	0.10	5.18	0.55	2.00
wmi	***wti3***	***lti3***	***lti4***	***wti4***	***wto4***	***msl***
0.10	0.27	0.73	0.63	0.35	0.68	6.50

power division is an equal T-junction power divider. The input GCPW transformed and equally divided in the first stage. In the second stage, power distribution is performed in the ratio 2:1 through unequal transformers. To feed the antenna element, a mode transformation from GCPW to SIW is performed using a transition based on the design in [35]. It is defined by the taper angle α and transition length ***lcs***. The total length of the feed network is given by ***gcpwl*** $= 5.18$ mm. The described feed network is designed and simulated. Simulation results are shown in Fig. 12. Due to the symmetric design transmission, coefficients only for output ports 2 and 3 are shown. It can be seen that a wideband performance is achieved with reflection coefficient remaining below -15 dB. Unequal power distribution is also achieved with transmission coefficients for the central ports being approximately 2.5 dB more than the outer ports.

C. Microstrip Feed Network

An MS power divider was also designed to feed the antenna array. Like the SIW and GCPW feed networks, a symmetric

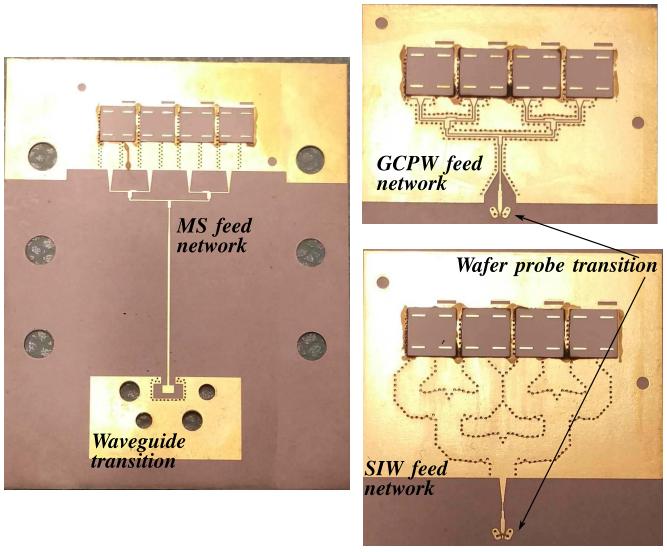

Fig. 14. Photographs of manufactured antennas.

design with two-stage power division was applied here as well. Similar to GCPW, the power division is performed here equally in the first stage, and unequally in the ratio 2:1 in the second stage. To feed the antenna element, the MS line is converted to SIW using the transition as shown in [36]. The taper length and width at SIW of this transition are ***lmt*** and ***wmt***, respectively. The total length of the power divider is given by the length ***msl*** $= 6.50$ mm.

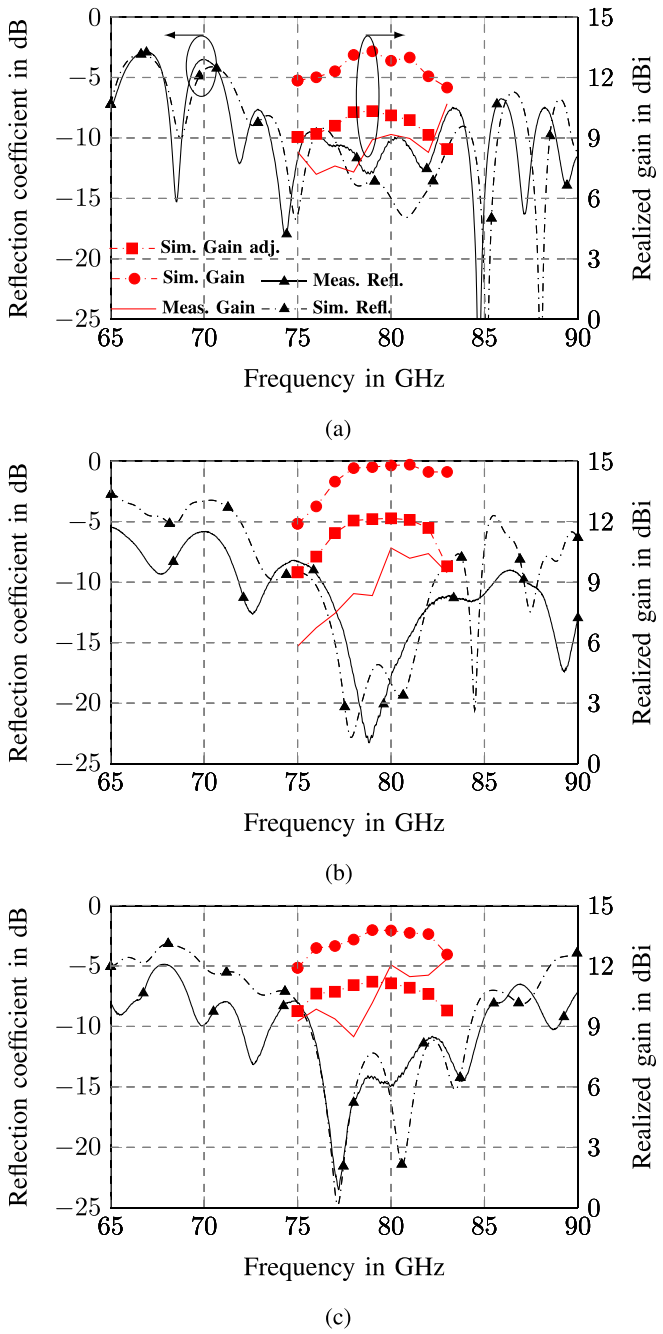

Fig. 15. Simulated and measured reflection coefficient and realized gain of antenna arrays. (a) SIW feed antenna. (b) GCPW feed antenna. (c) MS feed antenna.

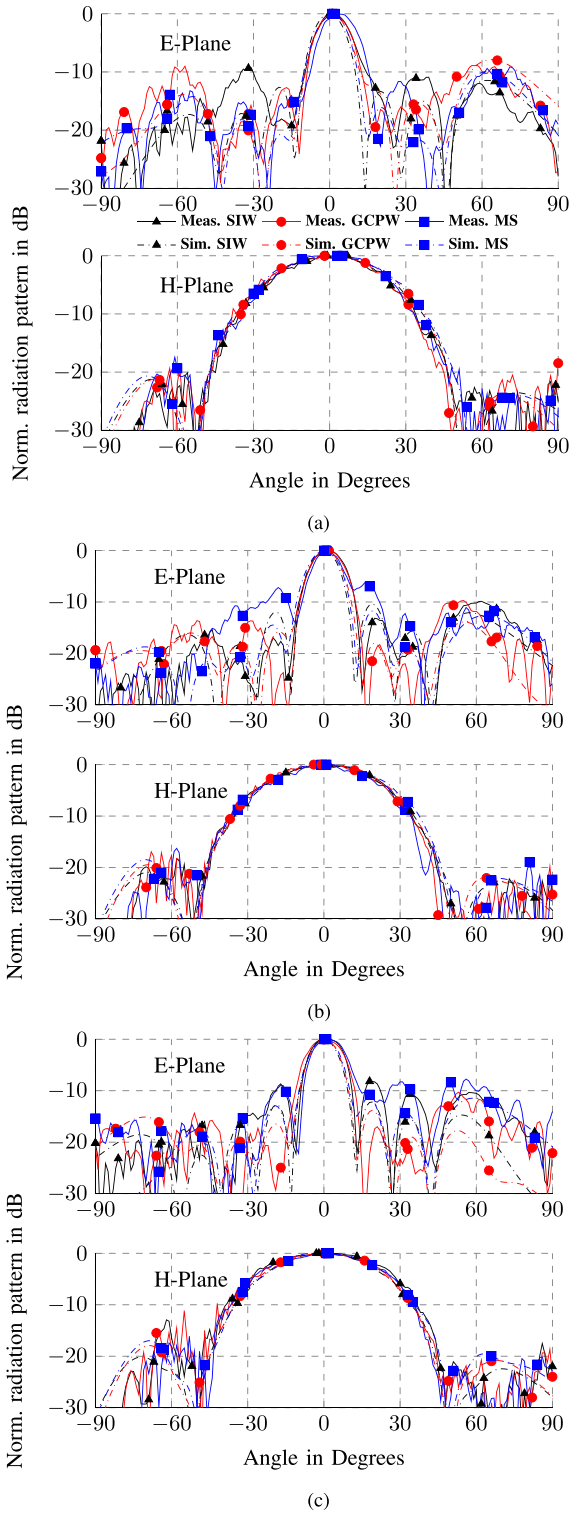

Fig. 16. Simulated and measured antenna radiation patterns at (a) 76, (b) 79, and (c) 81 GHz.

The designed model and the simulation results of the power divider are shown in Fig. 13. Due to symmetry, results are only shown for the output ports 2 and 3. It can be seen that a wideband performance is achieved with reflection coefficient remaining below -15 dB in the operating frequency range, and the transmission coefficients at the inner ports are, on average, 2.5 dB more than the outer ports.

V. Measurement Results and Discussion

The described antennas were manufactured and a subset is shown in Fig. 14. The same thin-film element is used in all the antenna arrays. The MS, GCPW, and SIW feed networks are also shown. Fig. 14 also shows two different transitions preceding the antenna feed networks to enable reflection coefficient and antenna pattern measurements, respectively. For the reflection coefficient measurements, an on-wafer probe setup was used. It consists of a vector network analyzer module PNA-X N5242A-based system whose output is connected to

TABLE III
COMPARISON OF THE PROPOSED DESIGN WITH REPORTED 60, 79, AND 95 GHz ANTENNAS

Ref.	Frequency (GHz)	Type	Number of elements	Size (mm^3)	Number of layers	Impedance bandwidth (%)	Gain (dBi)	Aperture efficiency (%)	Radiation efficiency (%)
[5]	60	Grid	4×15	15.0×15.0×0.6	3	9.6	17.7	59.9	n.a.
[9]	79	Grid	1×8	1.9×16.0×1.4	12	10.1	12.4	67.1	52.5
[10]	79	Slotted waveguide	4×4	10.8×7.0×0.1	1	10.7	11.0	19.1	38.0
[19]	95	Patch backed dielec. cube	4×4	30×20×2.6	3	7.7	18	n.a.	38.0
[16]	60	Cavity backed patch	4×4	17.4×12.3×2.1	4	22.6	19.6	80	54.5
Our work	79	Stacked double grid (SIW)	1×4	17.4×12.3×0.1*	1**	7.8	9.2	4.7	19.1
Our work	79	Stacked double grid (GCPW)	1×4	16.6×7.7×0.1*	1**	11.3	10.7	11.1	34.0
Our work	79	Stacked double grid (MS)	1×4	16.6×10.9×0.1*	1**	11.3	12.1	10.8	37.2

* Additional thickness due to thin film appr. 0.2 mm
** Thin films with two layers attached additionally at antenna positions

an on-wafer coplanar probe. In order to enable reflection coefficient measurements with the wafer prober, the antenna feed networks are preceded by coplanar MS transition. For the radiation pattern measurements, a waveguide-based measurement setup based on the HP 8360 Synthesized Sweepers [37] and additional frequency extenders was used. A waveguide to MS transition, based on [38] and adapted for an operating frequency of 77 GHz is used to connect the PCB to the measurement setup. This transition achieves a wide impedance matching bandwidth and a low maximum one way transmission loss of 0.45 dB [39]. For each type of feed network, samples with both types of transitions were manufactured.

A. Impedance Bandwidth and Broadside Gain

Fig. 15 shows the simulated and measured reflection coefficients and gains of the antenna arrays. Looking at the reflection coefficients, it can be seen that there is good agreement between the measured and simulated results for all feed networks. Measured reflection coefficient <-10 dB bandwidth for the SIW feed antenna is 7.8% (76.3–82.5 GHz), for the GCPW feed antenna is 11.3% (76.3–85.5 GHz), and for the MS feed antenna is 11.3% (75.7–84.8 GHz), respectively.

In terms of the realized gain, the measured values are lower than the simulated gain for all antenna types. Partially, this can be attributed to fabrication tolerances of the antenna and the alignment tolerances of the thin film on the PCB as well as the waveguide to MS transition that was used for the radiation pattern measurements. A large source of the discrepancy, however, is the difference in the PCB substrate loss tangent value of 0.0018 in the data sheet [40] and actual loss tangent values at 77 GHz. Actual values extracted from ring resonator measurements [41] show the loss tangent to be 0.01. The simulated gain using the adjusted loss tangent values is also plotted and they are much closer to the measured gain values.

Maximum measured realized gains within the frequency band 77–81 GHz occur at 80 GHz for all antennas. They are 9.2 dBi for the SIW feed antenna, 10.7 dBi for the GCPW feed antenna, and 12.1 dBi for the MS feed antenna, respectively. The difference in gain values between the feed networks can be attributed to the difference in losses due to the different sizes and transmission line modes of each feed network. The SIW feed network suffers the largest loss, because its length ***siwl*** is the largest. Even with a slightly shorter length of ***gcpwl***, the GCPW feed network also suffers larger losses than the MS feed network with length ***msl*** due to higher metallic losses caused by the additional coplanar ground planes. Gain values for all antennas remain within 3 dB of the maximum over the operating frequency band of 77–81 GHz except for the MS feed antenna at 78 GHz.

B. Radiation Pattern

A 1×4 linear array was designed in the E-plane with only a single element in the H-plane. Hence, a more directive beam is expected in the E-plane. The single thin-film element width is given by ***tfw*** $= 3.80$ mm. Including a 0.4 mm gap between the thin films, we obtain an interelement distance of 4.20 mm in the array. At the operating frequency of 77 GHz ($\lambda_0 = 3.90$ mm), this equals 1.07 λ_0. Due to the distance and the small number of elements in the array, higher sidelobes are expected.

Simulated and measured radiation patterns of the antennas are shown in Fig. 16. The results are shown for the frequencies 76, 79, and 81 GHz. A broadside main beam is measured in both planes. For the H-plane, the measured results agree well with the simulated values for the main beam and sidelobe levels. A 3 dB gain beamwidth of about 40° is measured in the H-plane, with a minimum sidelobe suppression of 18 dB over the operating frequency range for all feed networks. An exception to this is seen at 81 GHz, where sidelobes for

the GCPW feed network-based array increase for negative angles. For the E-plane, a 3 dB gain beamwidth of 12° is measured, and the main beam corresponds well with the simulated results for all feed networks. Higher sidelobes are seen in general for the measured radiation pattern compared with the simulated results. Differences in element height due to the adhesive can cause changes in coupling coefficients between the thin film and PCB. This would manifest itself as modifications in the weighting coefficients in the antenna array causing increased sidelobes. Second, due to the feed network radiation, which is present for MS and GCPW feed networks, an additional radiation component can deteriorate the antenna radiation pattern. Radiation efficiencies of 19.1% for SIW feed, 34.0% for GCPW feed, and 37.2% for MS feed network were obtained, respectively.

C. Comparison and Discussion

Key design and performance data of some recently reported millimeter-wave antennas at 60, 79, and 95 GHz are listed in Table III. Generally, larger array designs in terms of size and number of elements than the proposed design are realized at these frequencies. Mostly, such designs also employ multiple substrate layers. These are used to house the feed network below the antenna aperture for high gain and aperture efficiency [9] as well as stacked antenna elements to improve impedance bandwidth [16]. The proposed designs generally achieve lower gain and aperture efficiency due to a single layer structure, similar to [10]. The use of two-layer thin films allows a comparable impedance bandwidth to other designs, except [16], which achieves a larger impedance bandwidth. Although most multilayer designs employ SIW feed networks, for a single layer design, with the proposed antenna element, an MS feed network performed better than the SIW and achieved the best overall performance of the three designs.

VI. Conclusion

A new hybrid approach to designing multilayer antennas on single layer PCB in the millimeter-wave band for automotive radar was shown. Using thin-film elements that house the complete multilayer antenna structure, a new SIW slot fed stacked double grid antenna element was described. Using the thin-film antenna element, a 1×4 linear array was designed. To demonstrate the flexibility of the thin-film approach, array feed networks on the PCB were designed using SIW, GCPW, and MS transmission lines, respectively. Among the array antennas, the SIW feed antenna has an impedance bandwidth of 7.8%, and the GCPW and MS feed antenna have impedance bandwidth of 11.3%. A realized gain of 9.2 dBi for the SIW feed antenna, 10.7 dBi for the GCPW feed antenna, and 12.1 dBi for the MS feed antenna was measured. For all antennas, broadside radiation pattern with stable main beam is measured. These antennas can be used for medium- and short-range applications for automotive radar systems in the 77–81 GHz frequency band.

Acknowledgment

The authors would like to thank A. Kugler for his assistance in assembling the antenna structure.

References

[1] M. Li and K.-M. Luk, "Low-cost wideband microstrip antenna array for 60-GHz applications," *IEEE Trans. Antennas Propag.*, vol. 62, no. 6, pp. 3012–3018, Jun. 2014.

[2] W. M. Abdel-Wahab, S. Safavi-Naeini, and D. Busuioc, "Low cost 60 GHz millimeter-wave microstrip patch antenna array using low-loss planar feeding scheme," in *Proc. IEEE Int. Symp. Antennas Propag.*, Jul. 2011, pp. 508–511.

[3] J. A. G. Akkermans, M. H. A. J. Herben, and M. C. van Beurden, "Balanced-fed planar antenna for millimeter-wave transceivers," *IEEE Trans. Antennas Propag.*, vol. 57, no. 10, pp. 2871–2881, Oct. 2009.

[4] X. P. Chen, K. Wu, L. Han, and F. He, "Low-cost high gain planar antenna array for 60-GHz band applications," *IEEE Trans. Antennas Propag*, vol. 58, no. 6, pp. 2126–2129, Jun. 2010.

[5] B. Zhang and Y. P. Zhang, "Grid array antennas with subarrays and multiple feeds for 60-GHz radios," *IEEE Trans. Antennas Propag.*, vol. 60, no. 5, pp. 2270–2275, May 2012.

[6] S. Zhang and Y. P. Zhang, "Analysis and synthesis of millimeter-wave microstrip grid-array antennas," *IEEE Antennas Propag. Mag.*, vol. 53, no. 6, pp. 42–55, Dec. 2011.

[7] L. Zhang, W. Zhang, and Y. P. Zhang, "Microstrip grid and comb array antennas," *IEEE Trans. Antennas Propag.*, vol. 59, no. 11, pp. 4077–4084, Nov. 2011.

[8] F. Bauer and W. Menzel, "A 79-GHz resonant laminated waveguide slotted array antenna using novel shaped slots in LTCC," *IEEE Antennas Wireless Propag. Lett.*, vol. 12, pp. 296–299, 2013.

[9] F. Bauer, X. Wang, W. Menzel, and A. Stelzer, "A 79-GHz radar sensor in LTCC technology using grid array antennas," *IEEE Trans. Microw. Theory Techn.*, vol. 61, no. 6, pp. 2514–2521, Jun. 2013.

[10] S. Cheng, H. Yousef, and H. Kratz, "79 GHz slot antennas based on substrate integrated waveguides (SIW) in a flexible printed circuit board," *IEEE Trans. Antennas Propag.*, vol. 57, no. 1, pp. 64–71, Jan. 2009.

[11] M. Frei, F. Bauer, W. Menzel, A. Stelzer, and L. Maurer, "A 79 GHz differentially fed grid array antenna," in *Proc. 8th Eur. Radar Conf.*, Oct. 2011, pp. 432–435.

[12] O. Khan, J. Meyer, K. Baur, and C. Waldschmidt, "Substrate integrated waveguide slot-fed grid array antenna," in *Proc. Eur. Microw. Conf.*, Sep. 2015, pp. 1323–1326.

[13] D. M. Pozar, "Microstrip antennas," *Proc. IEEE*, vol. 80, no. 1, pp. 79–91, Jan. 1992.

[14] M. Li and K.-M. Luk, "A low-profile unidirectional printed antenna for millimeter-wave applications," *IEEE Trans. Antennas Propag.*, vol. 62, no. 3, pp. 1232–1237, Mar. 2014.

[15] R. B. Waterhouse, "Design of probe-fed stacked patches," *IEEE Trans. Antennas Propag.*, vol. 47, no. 12, pp. 1780–1784, Dec. 1999.

[16] Y. Li and K.-M. Luk, "Low-cost high-gain and broadband substrate-integrated-waveguide-fed patch antenna array for 60-GHz band," *IEEE Trans. Antennas Propag.*, vol. 62, no. 11, pp. 5531–5538, Nov. 2014.

[17] W. Han, F. Yang, J. Ouyang, and P. Yang, "Low-cost wideband and high-gain slotted cavity antenna using high-order modes for millimeter-wave application," *IEEE Trans. Antennas Propag.*, vol. 63, no. 11, pp. 4624–4631, Nov. 2015.

[18] D.-F. Guan, C. Ding, Z.-P. Qian, Y.-S. Zhang, W.-Q. Cao, and E. Dutkiewicz, "An SIW-based large-scale corporate-feed array antenna," *IEEE Trans. Antennas Propag.*, vol. 63, no. 7, pp. 2969–2976, Jul. 2015.

[19] N. Ghassemi, K. Wu, S. Claude, X. Zhang, and J. Bornemann, "Low-cost and high-efficient W-band substrate integrated waveguide antenna array made of printed circuit board process," *IEEE Trans. Antennas Propag.*, vol. 60, no. 3, pp. 1648–1653, Mar. 2012.

[20] Y. Huang, K.-L. Wu, D.-G. Fang, and M. Ehlert, "An integrated LTCC millimeter-wave planar array antenna with low-loss feeding network," *IEEE Trans. Antennas Propag.*, vol. 53, no. 3, pp. 1232–1234, Mar. 2005.

[21] Y. Li and K. M. Luk, "60-GHz substrate integrated waveguide fed cavity-backed aperture-coupled microstrip patch antenna arrays," *IEEE Trans. Antennas Propag.*, vol. 63, no. 3, pp. 1075–1085, Mar. 2015.

[22] Y. Li and K. M. Luk, "A 60-GHz wideband circularly polarized aperture-coupled magneto-electric dipole antenna array," *IEEE Trans. Antennas Propag.*, vol. 64, no. 4, pp. 1325–1333, Apr. 2016.

[23] Y. Li, J. Wang, and K. Luk, "Millimeter-wave multi-beam aperture-coupled magneto-electric dipole array with planar substrate integrated beamforming network for 5G applications," *IEEE Trans. Antennas Propag.*, to be published, doi: 10.1109/TAP.2017.2681429.

[24] M. Wojnowski *et al.*, "Embedded wafer level ball grid array (eWLB) technology for millimeter-wave applications," in *Proc. IEEE 13th Electron. Packag. Technol. Conf.*, Dec. 2011, pp. 423–429.
[25] Besi. *Datacon 2200 evo^{Plus}*. Accessed: Feb. 2, 2017. [Online]. Available: http://www.besi.com/fileadmin/user_upload/Datacon2200evoplus.pdf
[26] Henkel. *Loctite Eccobound FP5001*. Accessed: Jan. 21, 2017 [Online]. Available: http://na.henkel-adhesives.com/product-search-1554.htm?nodeid=8797729914881&msdsLanguage=EN_US&selectedTab=technical
[27] J. D. Kraus, "A backward angle-fire array antenna," *IEEE Trans. Antennas Propag.*, vol. AP-12, no. 1, pp. 48–50, Jan. 1964.
[28] R. Conti, J. Toth, T. Dowling, and J. Weiss, "The wire grid microstrip antenna," *IEEE Trans. Antennas Propag.*, vol. AP-29, no. 1, pp. 157–166, Jan. 1981.
[29] K. D. Palmer and J. H. Cloete, "Synthesis of the microstrip wire grid array," in *Proc. 10th Int. Conf. Antennas Propag.*, vol. 1. Apr. 1997, pp. 114–118.
[30] F. Bauer and W. Menzel, "A 79 GHz microstrip grid array antenna using a laminated waveguide feed in LTCC," in *Proc. IEEE Int. Symp. Antennas Propag.*, Jul. 2011, pp. 2067–2070.
[31] S. D. Targonski, R. B. Waterhouse, and D. M. Pozar, "Design of wide-band aperture-stacked patch microstrip antennas," *IEEE Trans. Antennas Propag.*, vol. 46, no. 9, pp. 1245–1251, Sep. 1998.
[32] Y. Uezato, H. Yoshitake, M. Shono, M. Fujimoto, and T. Yamawaki, "Compact and high-performance millimeter-wave antennas," *Fujitsu Ten Tech. J.*, vol. 36, no. 36, pp. 19–25, Jan. 2011. [Online]. Available: http://www.fujitsu-ten.com/business/technicaljournal/pdf/36-3.pdf
[33] J. Bechter, M. Rameez, and C. Waldschmidt, "Analytical and experimental investigations on mitigation of interference in a DBF MIMO radar," *IEEE Trans. Microw. Theory Techn.*, vol. 65, no. 5, pp. 1727–1734, May 2017.
[34] D. Deslandes and K. Wu, "Accurate modeling, wave mechanisms, and design considerations of a substrate integrated waveguide," *IEEE Trans. Microw. Theory Techn.*, vol. 54, no. 6, pp. 2516–2526, Jun. 2006.
[35] X.-P. Chen and K. Wu, "Low-loss ultra-wideband transition between conductor-backed coplanar waveguide and substrate integrated waveguide," in *IEEE MTT-S Int. Microw. Symp. Dig.*, Jun. 2009, pp. 349–352.
[36] D. Deslandes and K. Wu, "Integrated microstrip and rectangular waveguide in planar form," *IEEE Microw. Wireless Compon. Lett.*, vol. 11, no. 2, pp. 68–70, Feb. 2001.
[37] *HP 8360 Series Synthesized Sweepers User's Handbook Serial Numbers 83651B, 83630B*, 9th ed., Hewlitt Packard, Palo Alto, CA, USA, Nov. 1995.
[38] J. Machac and W. Menzel, "On the design of waveguide-to-microstrip and waveguide-to-coplanar line transitions," in *Proc. 23rd Eur. Microw. Conf.*, Sep. 1993, pp. 615–616.
[39] M. Frei, "Antennen fuer automobile Radarsensoren bei 79 GHz," Ph.D. dissertation, Inst. Microw. Eng., Univ. Ulm, Ulm, Germany, 2014.
[40] Rogers Corp. *RO3000 Series Circuit Materials*. Accessed: Dec. 15, 2016. [Online]. Available: https://www.rogerscorp.com/documents/722/acs/RO3000-Laminate-Data-Sheet-RO3003-RO3006-RO3010.pdf
[41] E. Topak, J. Hasch, and T. Zwick, "Compact topside millimeter-wave waveguide-to-microstrip transitions," *IEEE Microw. Wireless Compon. Lett.*, vol. 23, no. 12, pp. 641–643, Dec. 2013.

Osama Khan received the B.Sc. and M.Sc. degrees in electrical engineering from Jacobs University Bremen, Bremen, Germany, in 2010 and 2012, respectively. He is currently pursuing the Ph.D. degree, with a focus on investigating multilayer wideband antennas for millimeter-wave automotive radar, with the University of Ulm, Ulm, Germany.

From 2013 to 2016, he was a Ph.D. Student with Robert Bosch GmbH, Leonberg, Germany. Since 2016, he has been a Development Engineer with Robert Bosch GmbH, with a focus on designing planar antennas for automotive radar.

Johannes Meyer was born in Bremen, Germany, in 1982. He received the Dipl.-Ing. degree in electrical engineering and the Ph.D. degree from Leibniz Universität Hannover, Hannover, Germany, in 2009 and 2015, respectively.

In 2015, he joined Robert Bosch GmbH, Leonberg, Germany, as a Development Engineer. His current research interests include planar antenna design for automotive radar applications.

Klaus Baur received the Dipl.-Ing degree in mechatronic engineering from the Ulm University of Applied Sciences, Ulm, Germany, in 2007, and the Ph.D. degree from the Friedrich-Alexander University Erlangen-Nürnberg, Erlangen, Germany, in 2012.

From 2007 to 2012, he was a Research Assistant with the Ulm University of Applied Sciences within the Technology Project Radar on Chip for Cars. Since 2012, he has been with Robert Bosch GmbH, Leonberg, Germany, as a Development Engineer for 77-GHz antennas and automotive radar systems

Christian Waldschmidt (S'01–M'05–SM'13) received the Dipl.-Ing. (M.S.E.E.) and Dr.-Ing. (Ph.D.E.E.) degrees from the University of Karlsruhe (TH), Karlsruhe, Germany, in 2001 and 2004, respectively.

From 2001 to 2004, he was a Research Assistant with the Institut für Hochfrequenztechnik und Elektronik, University of Karlsruhe (TH). Since 2004, he has been with Robert Bosch GmbH, Leonberg, Germany, in the business units Corporate Research and Chassis Systems. He was heading different research and development teams in microwave engineering, RF-sensing, and automotive radar. In 2013, he returned to academia. He was appointed as the Director of the Institute of Microwave Engineering, University of Ulm, Ulm, Germany, as a Full Professor. He has authored or co-authored over 100 scientific publications and over 20 patents. His current research interests include radar and RF-sensing, mm-wave and submillimeter-wave engineering, antennas and antenna arrays, and RF and array signal processing.

Dr. Waldschmidt is currently the Vice Chair of the IEEE MTT-27 Technical Committee (wireless enabled automotive and vehicular applications), an Executive Committee Board Member of the German MTT/AP Joint Chapter, and a member of the ITG Committee Microwave Engineering (VDE). In 2015, he served as the TPC Chair of the IEEE Microwave Theory and Techniques Society International Conference on Microwaves for Intelligent Mobility. He is a reviewer of multiple IEEE transactions and letters.